Meteosat Third Generation : first AOCS in flight results from PFM-I1 LEOP and commissioning

L. Pirson[1], L. Ascani[2], S. Pessina[3], E. Cerone[4], G. Sechi[5]
[1]Thales Alenia Space, France, laurent.pirson@thalesaleniaspace.com
[2]OHB, Germany, livio.ascani@ohb.de
[3]EUMETSAT, Germany, Stefano.Pessina@eumetsat.int
[4]Telespazio, Italy, ernesto.cerone@telespazio.com
[5]ESA, Netherlands, Gianfranco.Sechi@esa.int

ABSTRACT

In December, the 13th 2022, the first Meteosat Third Generation satellite MTG-I1, aiming at renewing the current Meteosat fleet, was launched on Ariane5 from Kourou, French Guiana. It will be followed by three others MTG-I (Imaging) satellites and two MTG-S (Sounding) satellites between 2025 and 2033. The attitude control concept changes from spinning satellites, which was the selected approach for the first and second generations, to a three-axes stabilization, offering better pointing performances as requested by the new generation of Meteosat instruments.
This paper presents the AOCS architecture and the way it has behaved during the LEOP phase, including some lessons learnt for the next flight models. Then it introduces the first main results of the commissioning phase, notably the equipment and the FPM mode performance after instrument activation.

1. Introduction

The Meteosat Third Generation is an European project led by the European Space Agency for Eumetsat, it aims at renewing the current Meteosat fleet.
The whole mission is composed of 2 different spacecrafts : the MTG-Imager (4 Spacecrafts, Thales Alenia Space as industrial prime) and the MTG-Sounder (2 Spacecrafts, OHB as prime). The spacecrafts are collocated on a geostationary orbits.
The industrial sharing at AOCS level is the following one : Thales Alenia Space is in charge of the AOCS Fine Pointing Mode (“Normal” Observation Mode), OHB is in charge of the rest of AOCS (including equipment procurement and validation).
Both kind of spacecrafts have a similar platform including the AOCS design and equipment.
This common platform contains the AOCS equipments, two propellant tanks and some flexible appendages : one panel Solar Array on each Y SC face, one Ka Band Antenna on –X SC face, one DCS&GeoSar Antenna on + X SC face (MTG-I only).
The instruments are located on the + Z SC face oriented towards the Earth in observation mode.
Two Instruments are present on MTG-I SC :

- the Flexible Combiner Imager, successor of the MSG instrument, it will offer 16 channels between 0.3 and 13.3 microns, and deliver a full image of Earth every 10 minutes. It has been developed by Thales Alenia Space: this instrument contains notably a two-axis Scan Mechanism composed of a fork and a mirror. This mechanism allows to make the Instrument scanning the Earth thanks to a DC motor without having to change the Platform pointing.
- the Lightning Imager, manufactured by LEONARDO : a four optical camera instrument which aims to distinguish lightning signal from the much larger background signal (during the day) by discriminating between the two in a number of different domains,

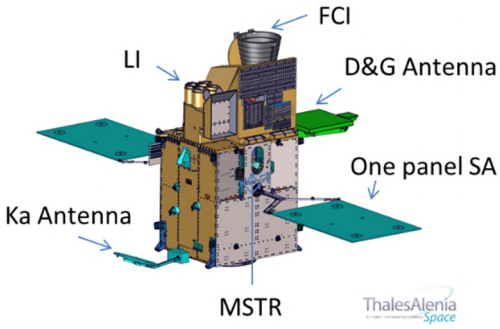

Figure 1. MTG-I

On MTG-S, two main Instruments are also accommodated :

- the Infra-Red Sounder which features a Fourier Transform Spectrometer (FTS) based concept (using the same scan mechanism than the FCI) offering hyper-spectral resolution in the thermal spectral domain,
- Ultraviolet Visible and NearInfrared Sounder, as part of the GMES Sentinal-4 mission

Thales Alenia Space leads the industrial consortium that is building the MTG family, with OHB as major partner.

The launch has been followed by a LEOP (Launch and Early Orbit Phases) period of 15 days led by EUMETSAT and TELESPAZIO from Fucino in Italy. EUMETSAT and Telespazio was helped by a ESA/Thales Alenia Space/OHB project support team. The handover to EUMETSAT has been achieved in the last days of 2022 after the spacecraft has successfully reached its position for in-orbit validation on geostationary orbit and has triggered the mode NOM/FPM (Fine Pointing Mode, very accurate Earth Pointing mode used to performed the observation). The satellite is now undergoing an eight months of commissioning activities whose objective is to assess the satellite and instruments functionality, operability and performance against the space segment requirements. It includes the payloads activation and operability using the Instrument Quality Tool(IQT).
The figure 2 shows a picture of the MTG-I1 PFM fully integrated in Kourou.

Figure 2. MTG-I PFM in Kourou

2. AOCS Overview

In the industrial MTG program sharing, OHB is in charge of the AOCS subsystem, including the AOCS equipment procurement, but Thales Alenia Space is responsible of the Fine Pointing Mode (Nominal Mode, with high pointing performances, in which the spacecraft will spend most of the time to perform the Earth Observation).
The AOCS, as part of the common platform used by both MTG-I and MTG-satellites has been designed to:

- support all the mission phases from release from the launcher to End of Life, controlling the attitude and the orbit,
- perform the transfer from GTO to GEO orbit, station acquisition, maintenance of the orbit, repositioning and disposal,
- support the operations of the payload and the data transmission to ground through High-data rate link,
- guarantee the operability and safety of the mission, in particular providing an independent and autonomous safe mode.

The set of sensor/actuators selected to realize all these activities are the following :

- 3 star-tracker (STR) AA-STR LEONARDO with Merging Software at quaternion level done inside AOCS SW,
- 1 gyroscope (GYRO) ASTRIX 200 from AIRBUS
- 5 reaction wheels (RW) from Rockwell Collins Deutschland with electrical torque up to 0.11Nm and angular momentum capacity of 45 Nms. Each reaction wheel is mounted on elastomer isolators used to filter the microvibrations exported by the RW towards the instruments,
- 1 set of 13 Cosine Sun Sensor Redundant (CSS) from Bradford, offering a full 360° coverture to find the Sun,
- 2 three-axis Coarse Rate Sensor (CRS) SiREUS from LEONARDO used exclusively by the Safe Mode (SRM), but staying ON and out of the loop in the other modes.
- 1 Sun Avoidance Sensor (SAVS) internally redundant from Toegepast Natuurwetenschappelijk Onderzoek (TNO) which ensure a hardware protection against Sun intrusion in FCI FoV.
- 16 10N bi-propellant Reaction Control Thrusters (RCT) by AIRBUS, providing full redundancy with respect to forces and torques. The thrusters are logically aggregated in 4 different sets (A,B,C and D) based on their position in the platform.
- 1 400N Liquid Apogee Engine (LAE) by AIRBUS to perform the transfer manoeuvres up to GEO orbit.

The Stand-by Mode (STBY) performs the initialization of units and unit drivers after launcher separation. It is used as well for on-ground testing activities.

The Sun Acquisition Mode(SAM) is- designed to acquire for all initial conditions a stable Sun pointing attitude. This is achieved by applying a control, that:

- Reduces high values of initial rotation (or initial angular momentum)
- Slews the S/C such that the –Z axis is pointing to Sun and the S/A is illuminated
- Enables and maintains a slow spinning of the S/C around –Z axis.

The SAM offers the possibility to use either a control on thrusters (named TSA) or a control on RW (RWSA) to avoid extra-fuel consumption when staying in Sun pointing.

The Guided Attitude Mode (GAM) is designed to achieve any kind of inertial pointing performing slow slews using RW. GAM is commanded with an attitude guidance profile, uploaded from Ground. It is used as an intermediate mode, to achieve defined target attitude, which are needed e.g. at the beginning of orbit transfer manoeuvres.

The Orbit Transfer Mode (OTM) gives the capability to perform the transfer to GEO, using the LAE. In nominal configuration a set of four thrusters on –Z satellite face is foreseen both for attitude control and as back-up to the LAE in case of failure and to perform slot acquisition/relocation/disposal. The mode keeps a guidance profile uploaded from Ground. Before and after the DV manoeuvre, the attitude control is performed using RWs to save fuel.

The Station Keeping Mode (SKM) allows orbit correction manoeuvres once in GEO (SKM N/S and SKM E/W) and RW unloading (SKM WO) to be performed using the RCTs. SKM uses a guidance profile generated on board using an Onboard Orbit Propagator (OOP). As for OTM, as soon as no DV manoeuvre or RW unloading are commanded, the attitude control is performed by RWs.

The Fine Pointing Mode (FPM) is the AOCS mode devoted to the Earth observation with payloads and thus offering the best pointing attitude and stability performances. The attitude estimation is based on a gyro-stellar estimator (using the merging of the 3 STRs and the GYRO measurements). The attitude is controlled with RWs, whose number and accommodation offer period of at least 21 days without any unloading need. Disturbances are limited either by design, rejecting them above the control bandwidths frequency (for instance Solar Array Drive Mechanism (SADM) with use of correct selection of microstepping frequency), by controlling them thanks to dedicated algorithm (as for wheel friction instabilities) or by using a feedforward mechanism to compensate a priori the disturbance torque generated by the main instrument mechanism (FCI 2 axis Scanning Mirror Mechanism (SCAN)).

Lastly, the Survival Mode (SRM) performs a fully autonomous stabilized and robust Sun acquisition and pointing in case of critical failure, . The SRM implementation is separated from other AOCS equipment and is as much as possible independent. It uses the redundant CSS cells, both CRS units, a redundant set of the RCTs and the redundant Processor Module (PM-B). Further on it applies different SW functions (use of specific code branches).

The AOCS units, i.e. sensors and actuators used by AOCS to accomplish the foreseen tasks and their usage in each AOCS mode are reported in the Table 1.

	CSS	STR	GYR	RWA	RCT	LAE	CRS
STBY	(X)	(X)	(X)	(X)	(X)		(X)
SAM(1)	X		X	X	X		
GAM	(X)	X	X	X	X		
OTM	(X)	X	X	X	X	X	
SKM	(X)	X	X	X	X		
FPM		X	X	X			
SRM	red				red		X

(X) Only for initialisation, monitoring and test purpose
SAM [1] The activated submode of SAM uses a subset of the assigned equipment
red The redundant units are used (exclusively for SRM)

Table 1. HW vs AOCS mode matrix

More details about AOCS design and algorithms can be found in reference [1], [2], [3].

3. LEOP Phase

3.1 Separation and Sun acquisition

MTG-I1 was successfully launched on Tuesday, December 13th, 2022 at 20:30 UTC, with Ariane 5 launcher from Europe's Spaceport in Kourou, French Guiana.
The operation during LEOP phase were driven by TELESPAZIO from their control centre located in Fucino from December, the 13th to December the 28th.
During the LEOP phase, the AOCS was exercised starting from the autonomous separation sequence, where, after the unit initialization, the first attitude slew to Sun acquisition has been commended on the redundant chain in SRM. The reconfiguration was triggered by an over-zealous FDIR threshold on the pressure after priming. In this failure scenario, being the back-up RCT close to the stowed SA panel, the thrusters must be commanded by the AOCS algorithm with a limited duty cycle (i.e., maximum 35%). The Sun acquisition manoeuvre and Sun pointing control was performed according to the prediction in terms of agility (180° slew in less than 8 minutes with 35% duty cycle) and maximum attitude control error always below 20°. In the following attitude control error angle is always defined as difference between the target attitude and the on board estimated attitude.
Please not that in between the 2 slews reported in the Figure 3, there is a phase of free drift where the Solar Panels are deployed.

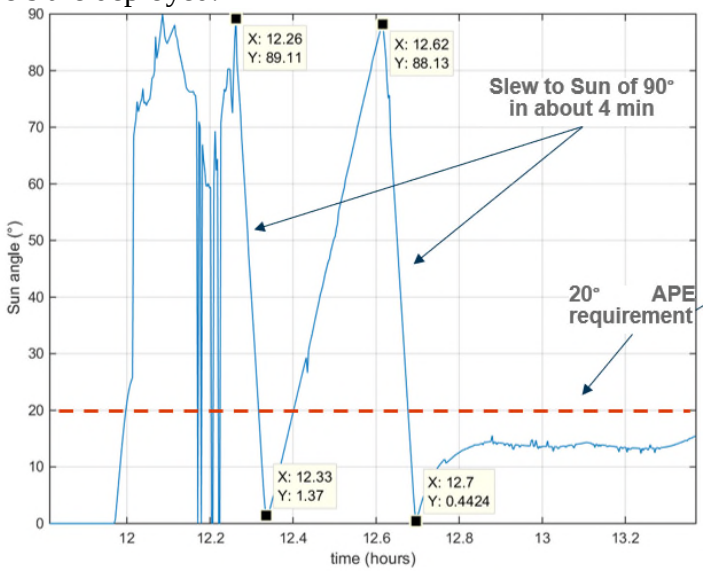

Figure 3. Sun pointing error during Separation Sequence (Survival Mode)

After return to Nominal chain the AOCS mode has been commanded to SAM with thrusters (SAM/TSA). In this mode have been carried out all the early operations performed on the satellite until the RWs initialization (RW run-in to reach the acceptable loss torque levels). The SAM/TSA shows an agility in line with the simulation results: maximum re-orientation of 180° in less than 4 minutes, maximum pointing error around 11° and steady-state consumption of 6 gr/hour. During the eclipse phases (in the Figure 5 with red curve) the Sun vector is precisely propagated using the GYRO data, so that at exit from eclipse period (about 30 minutes of umbra) the pointing error remains around 11° and no slew is necessary to acquire the Sun pointing.
During 6 hours of RW run-in the disturbance torque increases and keeps the pointing error close to the dead-band limit of 11° and also the fuel consumption increases (see section 4.4 for run-in effectiveness and results discussion).

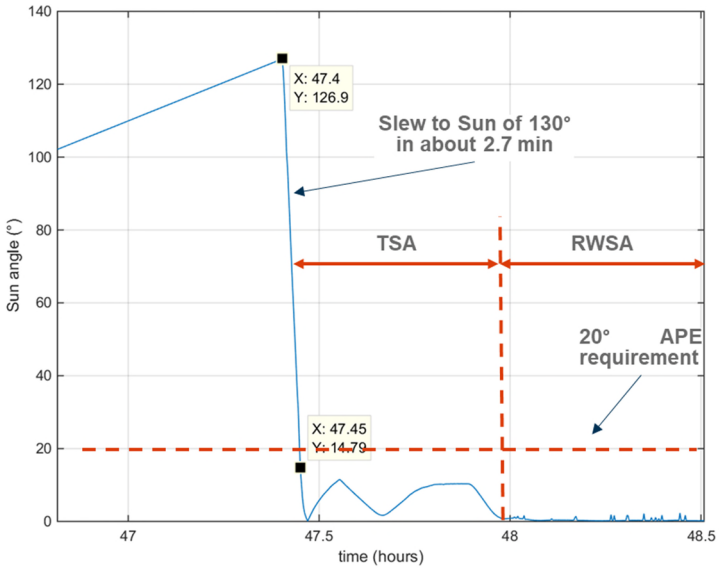

Figure 4. Sun pointing error during slew and steady-state in SAM

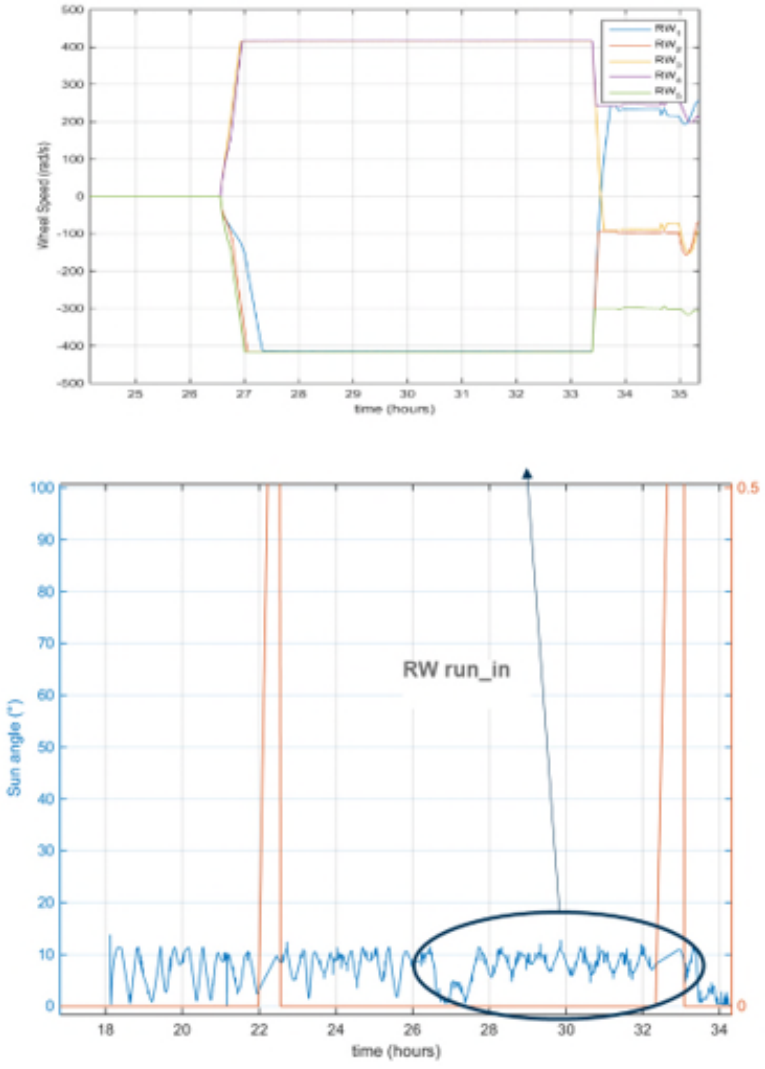

Figure 5. Sun pointing error (bottom) and RW speeds (top) in SAM/TSA

After RW run-in the wheels have been used to keep the Sun pointing in SAM, with an accuracy of maximum 3° and a re-orientation capability of 90° in less than 10 minutes.
The pointing accuracy of maximum 3° has been verified by using the STR as reference, as shown on figure 6.

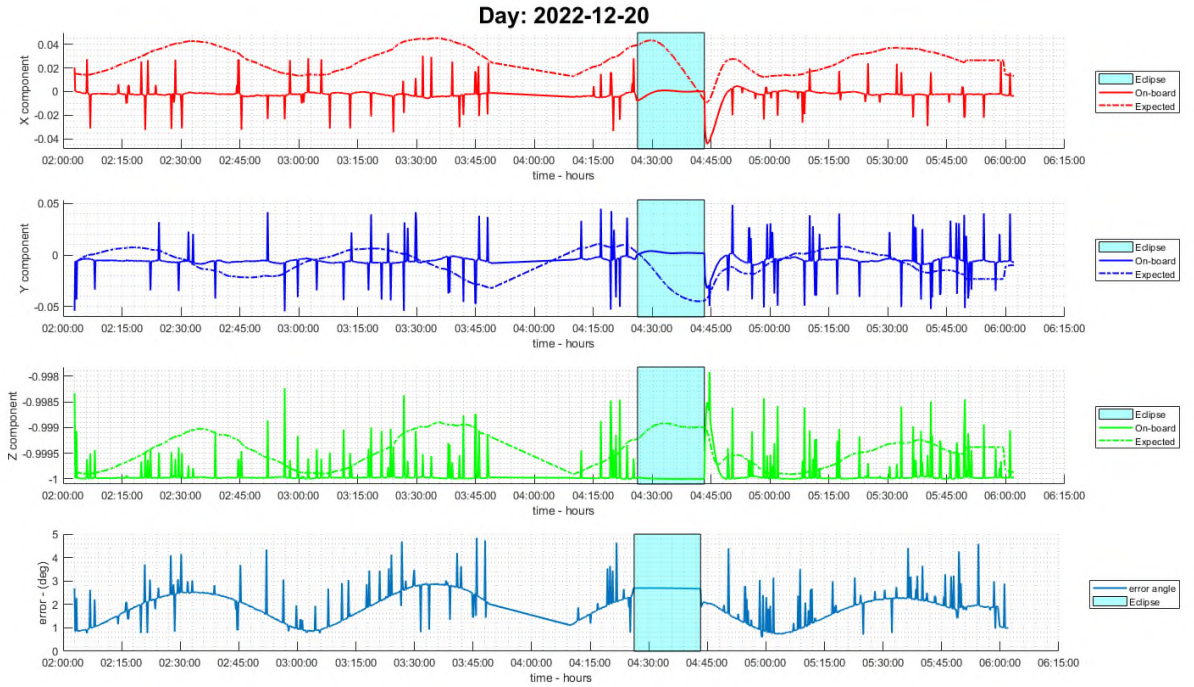

Figure 6. Sun pointing error during SAM/RWSA wrt STR attitude measurement

3.2 From GTO to GEO - Apogee Motor Firing and Station Acquisition manoeuvres

GAM has been entered during LEOP to prepare the Apogee Motor Firing (AMF) manoeuvre and the entry to FPM mode at the end of the phase. The total time to perform the attitude slew from Sun pointing to firing attitude was always below the 1 hour requested by requirement (including 20 minutes of spin rate dumping and quaternion initialization), while the pointing error well below the 0.16° requirement per axis (less than 200 arcsec at acceleration change and less than 10 arcsec during the coasting). The SADM start and stop to reach the reference position before the AMF is also producing an angular error of about 25 arcsec. This is shown on figure 7.

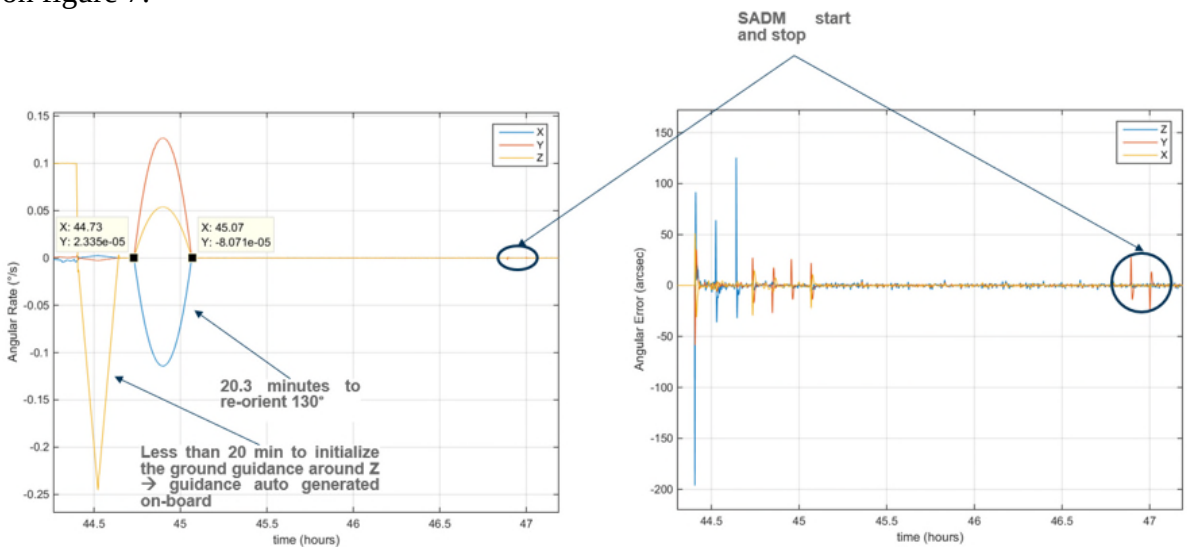

Figure 7. S/C rates (left) and angular error (right) during GAM

The orbit raising strategy to reach the GEO commissioning longitude slot at 3.4° +/-0.3° West from the GTO was planned to be based on 4 Apogee Motor Firings (AMF) , 3 main burns and 1 minor trim (by using the LAE), followed 3 small corrections manoeuvres (done with RCTs)
The GTO to GEO transfer has been successfully implemented, despite the AMF1 was interrupted after 400 seconds of LAE ignition due to the attitude failure detected by the AOCS SW when the angular error exceeded 2° during the steady-state phase. The orbit raising plan was completed with 3 longer AMFs (removing, the need of a final LAE trim manoeuvre, to preserve the LEOP timeline), after adaptation of the attitude FDIR threshold and re-computation of Flight Dynamics products.
From the attitude control point of view each AMF showed a similar behaviour with angular de-pointing up to 2°, thus exceeding the maximum steady-state error studied during the design phase of 1°. The initial overshoot due to the LAE activation was always below 7° for all the 4 AMFs, this being well in line with the results obtained with the simulation campaign (maximum overshoot of 15°). In the Figure 8 and 9, the AMF3 is reported as exemplary manoeuvre.

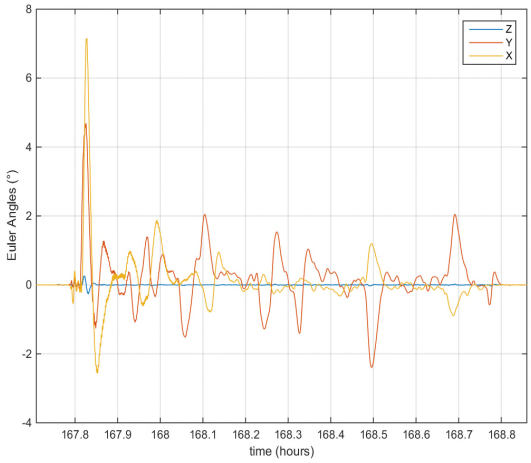

Figure 8. Angular error during AMF3

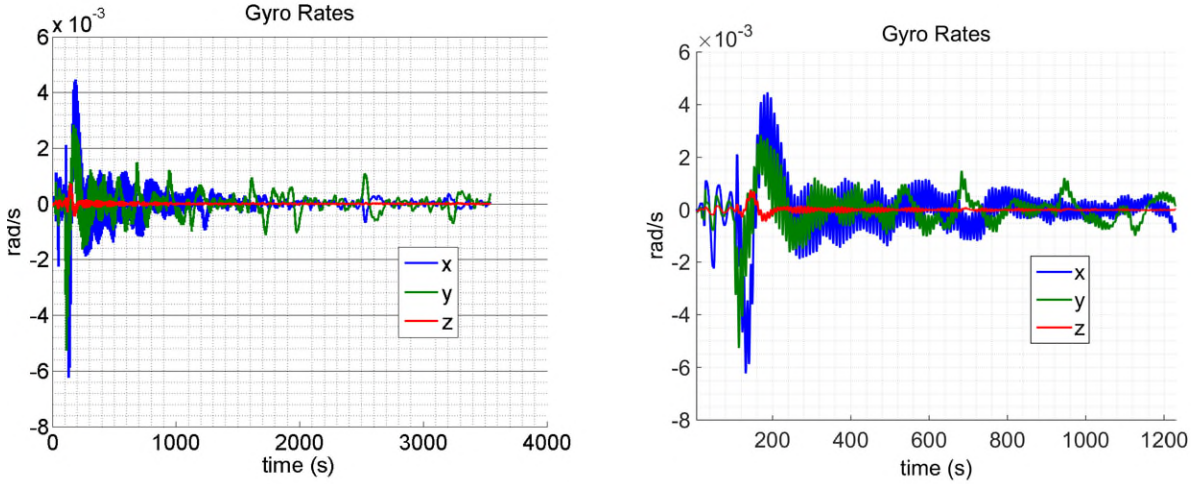

Figure 9. S/C rates (left) and zoom (right) during AMF3

By reconstructing the disturbance torque from the gyro data and from the thruster history log collected at 10 Hz it is observable the damped oscillation due to the fuel sloshing (this is happening at around 0.11 Hz as expected) and sporadic disturbances with the shape of steps, always in the same direction and amplitude (i.e. about 0.5 Nm), mainly around Y axis. These steps were not modelled during the design phase and are responsible of the higher de-pointing observed during the manoeuvre. The root cause is still under investigation but can be

compatible with a variation of the thrust vector of 0.05° or a static change of S/C Centre of Gravity position of few millimetres.
It is also possible to note the modulation of the amplitude of the disturbance torque due to a slightly different fuel oscillation frequency inside the two tanks.
This is better understandable by observing the Power Spectral Density (PSD) of the 10Hz rate data (below). The two peaks at around 0.11 Hz are the first mode of each propellant tank (0.10878394 Hz and 0.1160362 Hz respectively according to the pendulum model provided by tank supplier, within the range considered during the design phase,. This causes a beat at around 0.0110 Hz, visible in the amplitude modulation in the Figure 10. The control bandwidth in the order of 0.01 Hz has been correctly placed to avoid excitation of the first sloshing mode. Depending on final conclusion, the control tuning for next FMs will be probably reviewed with small increase of the bandwidth.
The first Solar Array mode is also clearly visible around X, but at a frequency higher than the one considered during the design (0.75 Hz, above the range of 0.4-0.6 Hz). This is anyway a common approach to provide more conservative ranges for the design of the attitude control.
The RCT actuation every 300 ms for attitude control is finally observable at 3.33 Hz.

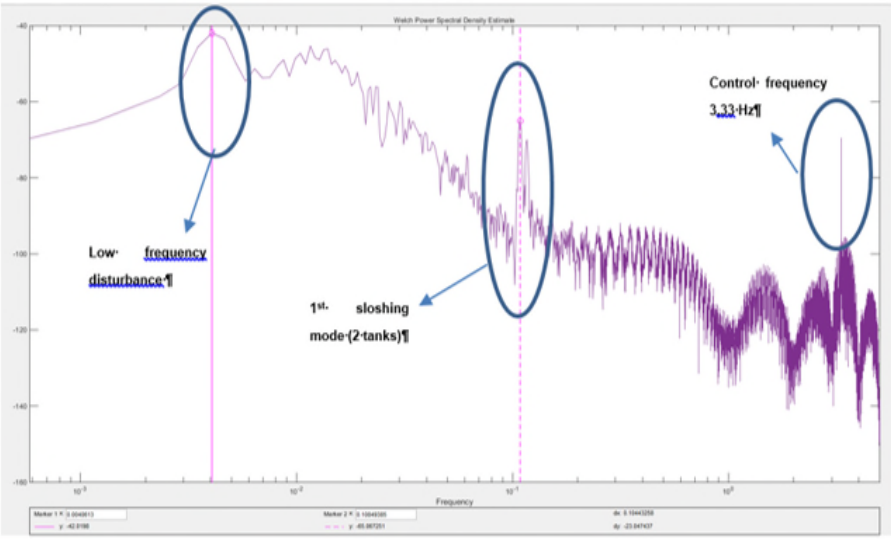

Figure 10. S/C rate Y axis PSD in dB

From the orbit correction point of view, the AMFs have confirmed the efficiency resulting from the AOCS simulation campaign to be above 99.5%. This led to an overall satisfactory performance in terms of delta-V budget and fuel consumed to arrive in the GEO slot.
This is confirmed from the 1.7 m/s delivered along the non-desired direction, to be compared with 506.6 m/s of orbit correction, this leading to 99.7% dV efficiency.
The larger attitude control error observed during AMFs (as for Fig. 8) did not prevent to meet the actual requirement for the manoeuvre execution, since mainly the average de-pointing error is relevant.

The orbit raising strategy was completed with 3 Station Acquisition manoeuvres (STAQ) to circularize the orbit at the GEO altitude and enter in the desired longitude slot. These corrections have been performed in OTM with RCT only. The manoeuvre accuracy was always well inside the maximum deviation considered during the design phase of 1°, with a maximum angular error smaller than 0.2° (see the result of the STAQ2 on figure 11).

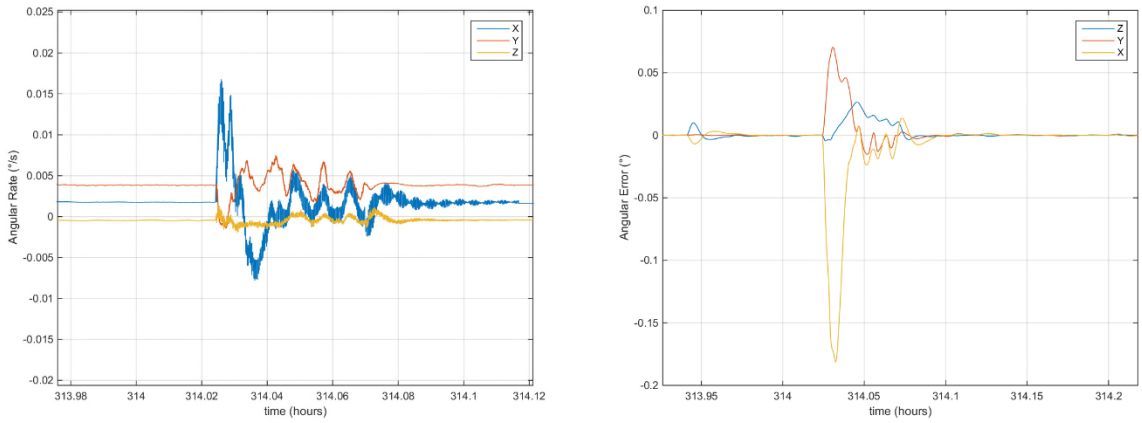

Figure 11. S/C rates (left) and angular error (right) during STAQ2

Also in terms of delta-V accuracy the efficiency was always above 91% considered in the propellant budget (94% for STAQ2).
Each manoeuvre were followed by a quite complex calibration activities involving all the FD/AOCS and Unified Propulsion System (UPS) teams. Thanks of that, it was possible to release the satellite at the end of the LEOP phase at the specified longitude (3.4W) with an error below 0.1% (well inside the allowed slot).

After successful both antennas deployment, LEOP phase is terminated by the transition to FPM which is described in the fifth part of the article.

4. Behaviour of AOCS equipments during LEOP and early commissioning

Here we will focus on main results observed on AOCS equipments, note that for what concern the CSS, there is nothing special to report, behaviour is as expected.

4.1 Coarse Rate Sensor (CRS)

The CRS is known to have a bias that can vary significantly depending on notably temperature conditions or after switch OFF/ON sequence (charge strapping effect). That's why, it was decided to calibrate them a last time in Kourou less than two months before the launch. Bias was calibrated waiting for complete thermal stabilization after power on and by taking mean value over 1hour. New bias values were then upload in the CRS EEPROM.
After the launch, CRS shows a quite good bias stability and mean value over one day does not request any re-calibration before May.
Figure 12 shows a typical pattern of satellite rate measured by the CRS B channels at end of March after 3 months in orbit without calibration; satellite is in FPM, slowly rotating at Earth rate. Only Z-axis reaches a bias level close to 90deg/hr, limit fixed for requesting recalibration. The temperature is also plotted on figure 13, allowing to see the correlation with bias.

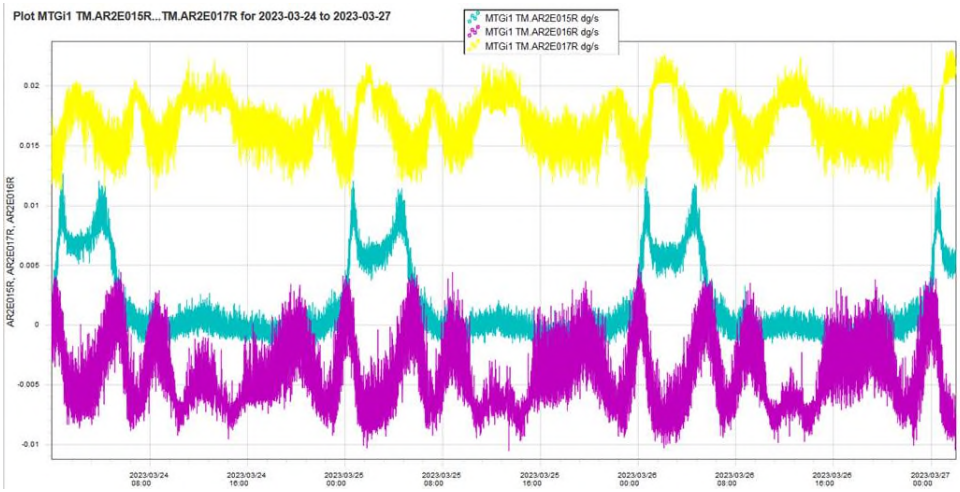

Figure 12. CRS-B measured in FPM respectively along X, Y, Z CRS axis

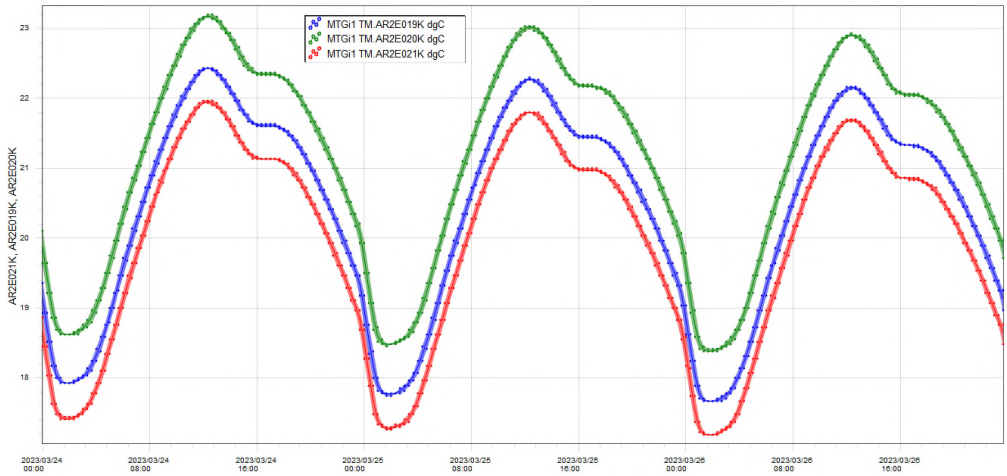

Figure 13. CRS-B PCB measured in FPM along X, Y, Z CRS axis

A specific on-ground algorithm based on mean measurement values over one complete day compared to reference provided by GYRO measurement is used to calibrate and upload on board the new bias.

4.2 Fine Gyroscope

On GYRO side, the measurement accuracy is very good and as expected. Since they are quite sensitive to microvibration, the GYRO assembly has been mounted on a damper to increase its robustness to microvibration: this works well since there was no observation of loss of measurement , notably during the phases of appendages deployment (Solar Arrays, Antennas, Instrument Baffle Cover) with pyro shocks although it was kept ON. There is neither any observed sensitivity to resonance of RW modes at specific speeds for the moment.
However the GYRO damper was regulated at 20° thanks to heater used in PWM. Temperature was selected to ensure best filtering characteristics of the elastomer. The activation of this thermal regulation loop on cycle of 10sec creates a non-expected disturbance on attitude control error whose amplitude varies with the heater activation duty cycle (DC). Some in flight tests prove that the disturbance disappear when heater is always ON or always OFF, or when the heater set point is reduced to 10° (thus reducing the steady state value of the duty cycle) as shown in figure 14.

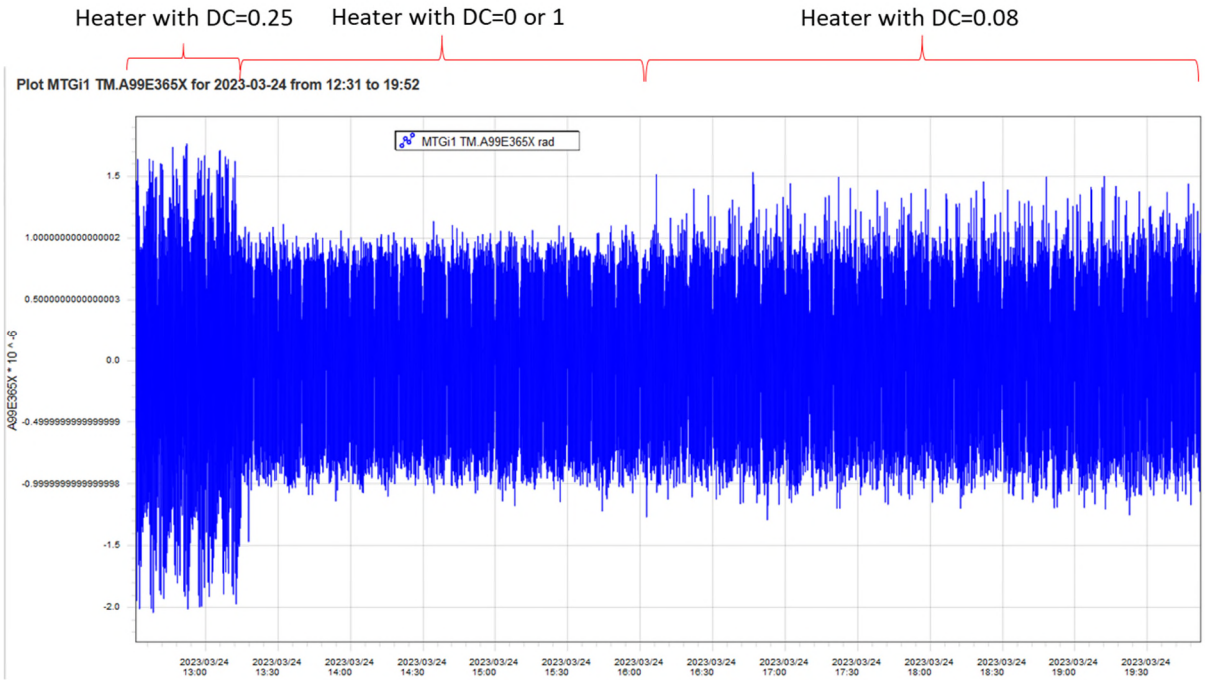

Figure 14. Impact of gyro damper heater on attitude error

4.3 Star-Tracker

The three STRs from LEONARDO show also a good behaviour. The correct autonomous management of the available STR heads by the merging software has been tested. In addition this merging software also estimated and corrected the misalignment between the LoS of the different STRs thanks to a Kalman Filter. The objective is to capture the seasonal evolution due to thermoelastics effect so the bandwidth of the Kalman filter is very low, thus avoiding to be sensitive to STR measurement noise. Note that by design, thermoelastics are quite reduced since the three STRs are mounted on a same very stable mechanical structure (Star Tracker brackets).

4.4 Reaction Wheel

At RW level, in the first days of LEOP after a RW run-in phase (RW spent several hours at 4000rpm in order to stabilize the lubrication of the ball bearing), the global values of the RWs friction were checked, one reaction wheel show a friction a little bit higher than expected (above30mNm at max speed, see RW1 on figure 15) even after a quite long run-in but without any consequence on the design and performance (still higher but very stable for this RW).

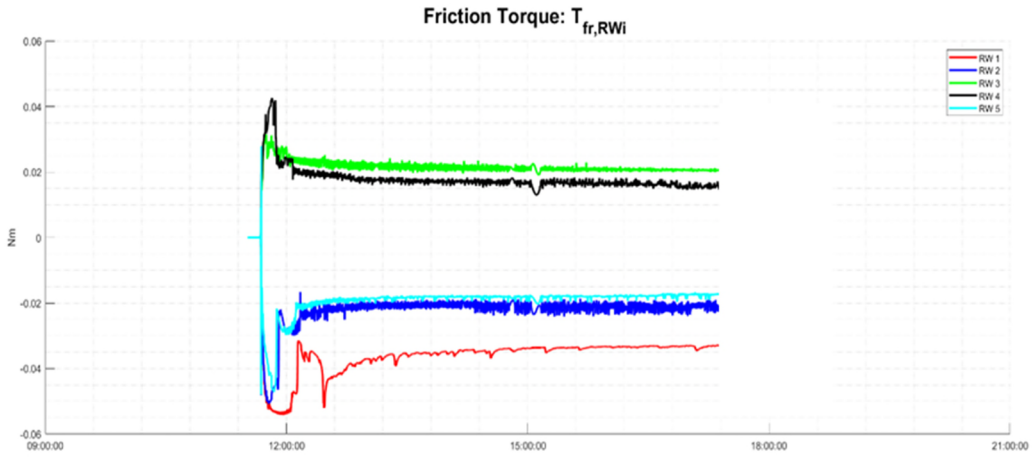

Figure 15. RWs friction during Run-in phase

No other suspicious behaviour was observed on the RW while in LEOP. Once in FPM, thanks to a very accurate optimized algorithm to estimate reaction wheel speed, the software is able to estimate and compensate with a quite high bandwidth (largely superior to the attitude control one) the friction of each RW and its potential variation (as typically the loss torque jumps). Lots of different kinds of friction jumps were noticed on several different wheels since the satellite reached FPM for the first time, but thanks to the efficiency of the wheel friction compensation algorithm, no significant impact on attitude control is observed: this is an important feedback for future fine pointing missions.
On the figure 16 is shown an example of the estimated wheel friction torque for the 5 RWs while in FPM: behaviour is not really similar from one wheel to the other and today there is no evident correlation between speed and friction jump or friction noise.

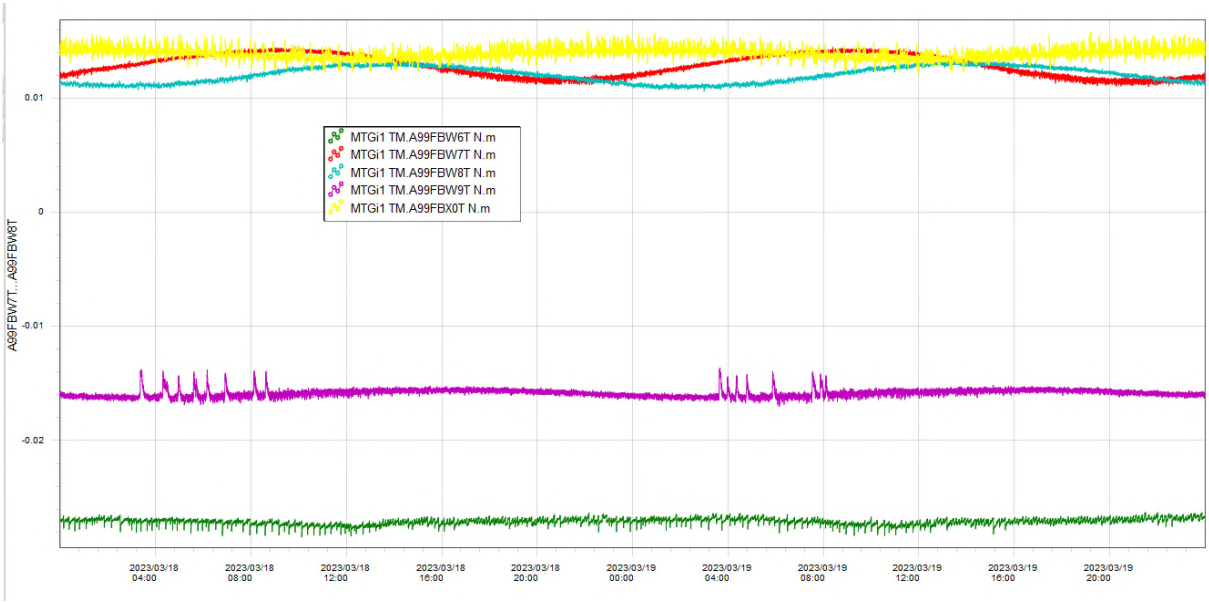

Figure 16. RWs friction estimated in FPM

5. First Feedback on MTG Nominal operation

5.1 Transition from SKM to FPM

The FPM is entered for the first time on December, the 27th. The transition from SKM is quite smooth as expected since attitude estimation and wheel control management function are functions shared by these two modes. The figure 17 illustrate this transition (SAQ and NOM modes are the satellite modes, NOM corresponding to SKM or FPM AOCS modes) : starting to Sun pointing in SAM, then transition to GAM to reach the Earth pointing, then transition to SKM with RW unloading before finally triggering the FPM.

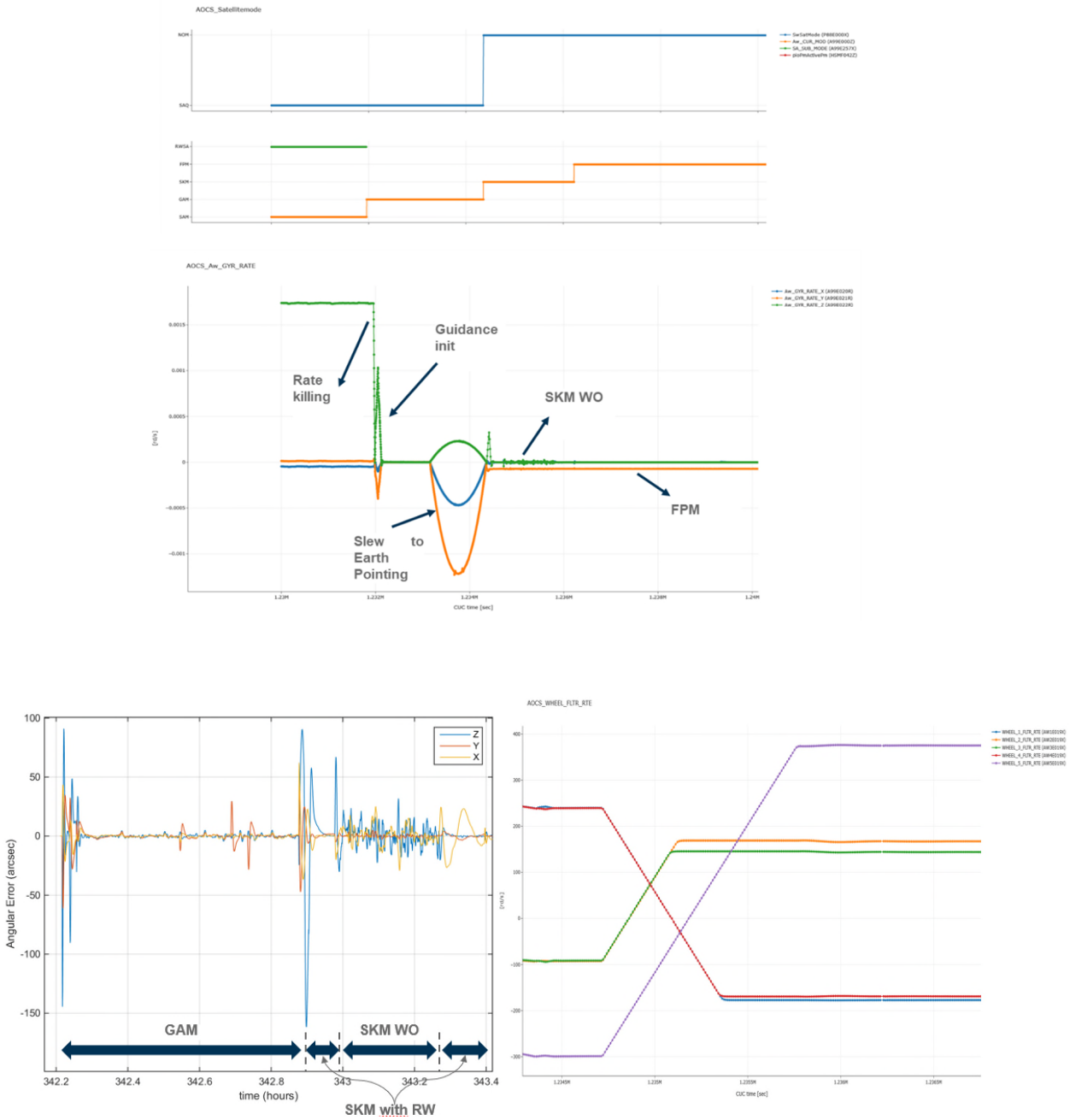

Figure 17. First transition to FPM: rate, attitude error and RW speeds evolution

Prior entering FPM, the OOP was initialized by the ground and populated by polynomial coefficients as computed by the ground based on ranging estimation. The guidance transition

from GAM (target fully computed by ground and uploaded) to SKM (target computed by OOP) was smooth, confirming at first view the correct behaviour of the OOP.
The MTG OOP is based on a harmonic and polynomial approximation of a geostationary orbit based on coefficient upload from ground (Clohessy-Wiltshire equations), nominally one time per day. Then this OOP will compute two targets quaternions: for the estimated Local Orbital Frame used by SKM for orbit correction manoeuvre, and for the estimated Earth Pointing Target Frame, used by FPM to point a selected fixed point on the Earth (which can be thus different from Nadir). The transition from one to the other is performed in SKM (after triggering from FPM and then after the manoeuvre before coming back in FPM).
The OOP has demonstrated its robustness in flight notably at each update from ground: a filtering allows to smooth the guidance step at daily update, avoiding any visible transition on attitude control error.

At the beginning the FPM is used without any activation of the instruments and thus no disturbance created by the FCI SCAN. The attitude control error in this configuration is very good (below 1µrad along each axis although the global pointing requirement is at 96µrad).
While in FPM, these are the RWs which accumulate the external disturbances mainly created by the solar pressure. The initial RW speeds, given as target to SKM for RW unloading prior FPM entry, were computed based on analysis of the effect of a priori solar pressure and gravity gradient estimation: objective is to maximize the duration between two unloadings, reaching typically one month (could be more around equinox where solar pressure torque is lower). Unloading is not requested while RWs speeds stay between 62.8 rad/s (minimal speed to use the very accurate RW speed estimation) and 418 rad/s (max nominal RW speed on MTG). Unloading can then be realized as a stand-alone operation in SKM without creating any DV or in a more optimized way when performing some NS orbit correction manoeuvre (since unloading requests duration of several hundreds of seconds, it is not possible to do it during EW manoeuvres which are very short ones (below 100seconds)).
On figure 18 is plotted an example of 5 RWs speeds evolution over 3 days.

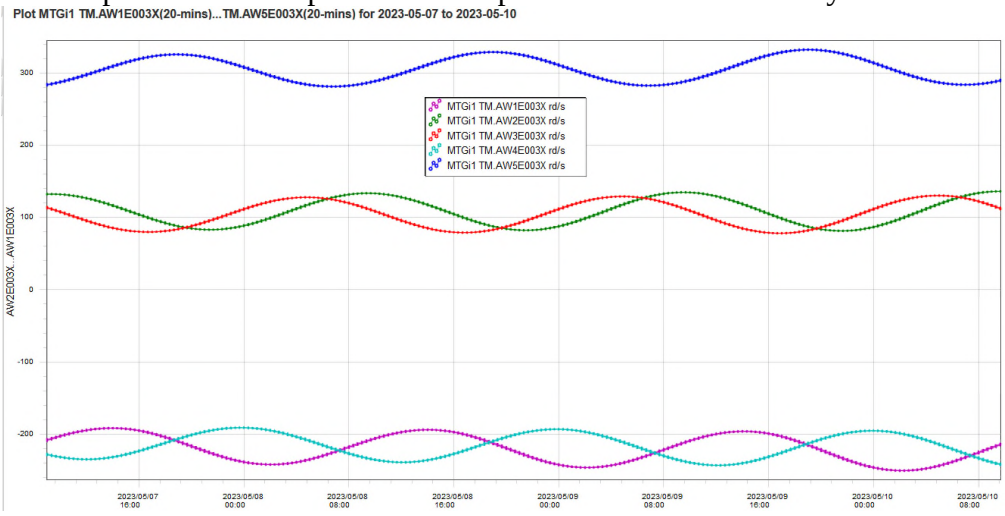

Figure 18. RWs speeds evolution in FPM over 3 days (RW1 to RW5)

5.2 SKM E/W

Then to keep the spacecraft on its orbit longitudinal window, it was requested to perform an EW manoeuvre : the delta-V of 0.055m/s is created by a dedicated thruster used in open-loop and located on the X face of the spacecraft, while four others thrusters ensured the attitude control during the manoeuvre. In order to limit the disturbance torque of the dedicated thruster,

a force factor of 0.3 is applied, even with that, the manoeuvre is very short, less than 40seconds, as a result, at the end of the manoeuvre, when the control is switched from RCT back to RW, it is still in transient phase, this creates a new transient on attitude error (even more important that the one at start of the manoeuvre). However thanks to extended FDIR thresholds, the attitude reconverges properly up to autonomous transition to FPM. This is shown on figure 19

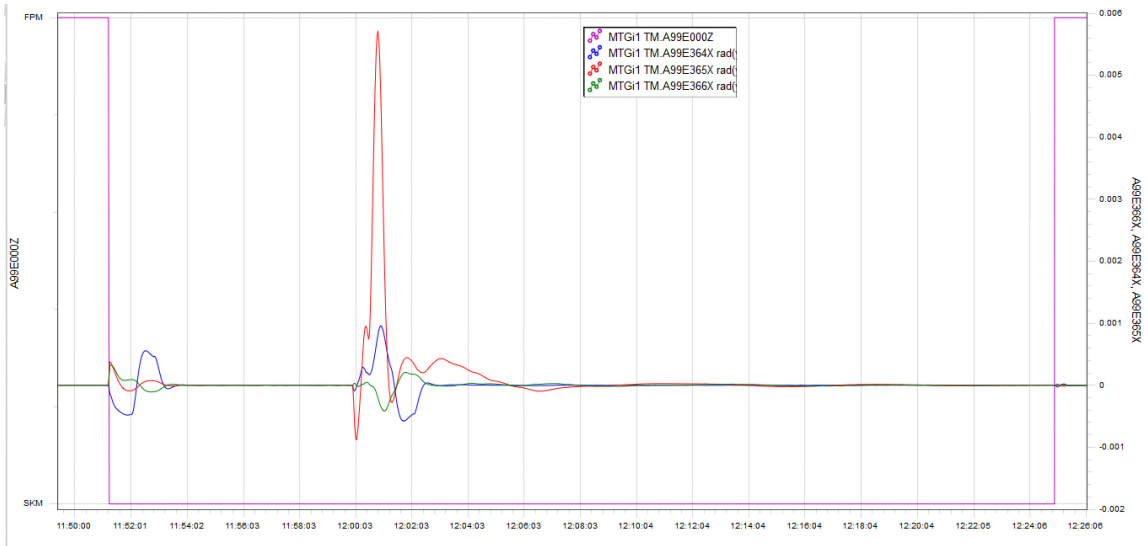

Figure 19. Attitude control error along the 3 sat axis during the EW manoeuvre (A99E364 = Z sat axis, A99E365 = Y sat axis, A99E366 = X sat axis)

5.3 FPM with FCI scanning

To scan the Earth, since MTG is now a three-axis stabilized Earth pointed spacecraft, the scanning mirror of the FCI is mounted on a two-axis SCAN mechanism allowing to perform a Full Earth Disk scanning in 600seconds, following 70 East/West swaths. The kinematics of this movement will create some disturbances on attitude and could also excite bending modes of the satellite appendages. As a result, since the SCAN movement is too fast to be managed by classical AOCS attitude control bandwidth, its effect is counteracted by the use of A-Priori Compensation (APC) torque, stored on board in a SW look-up table, and send in feedforward to the attitude controller: this requires of course to know a priori the movement of the SCAN and also the synchronization between SCAN movement and PF RW commanding.
Before enabling this APC, the good behaviour of SCAN control law performances has been checked : after correction of the encoder harmonics error (encoder being the sensor used by the scan control loop: its measurement is corrupted by a spatial noise pattern that is mostly reproducible and which can then be removed once it has been properly characterized), the scan control error is very good : below 5µrad along both axis as shown on figure20.

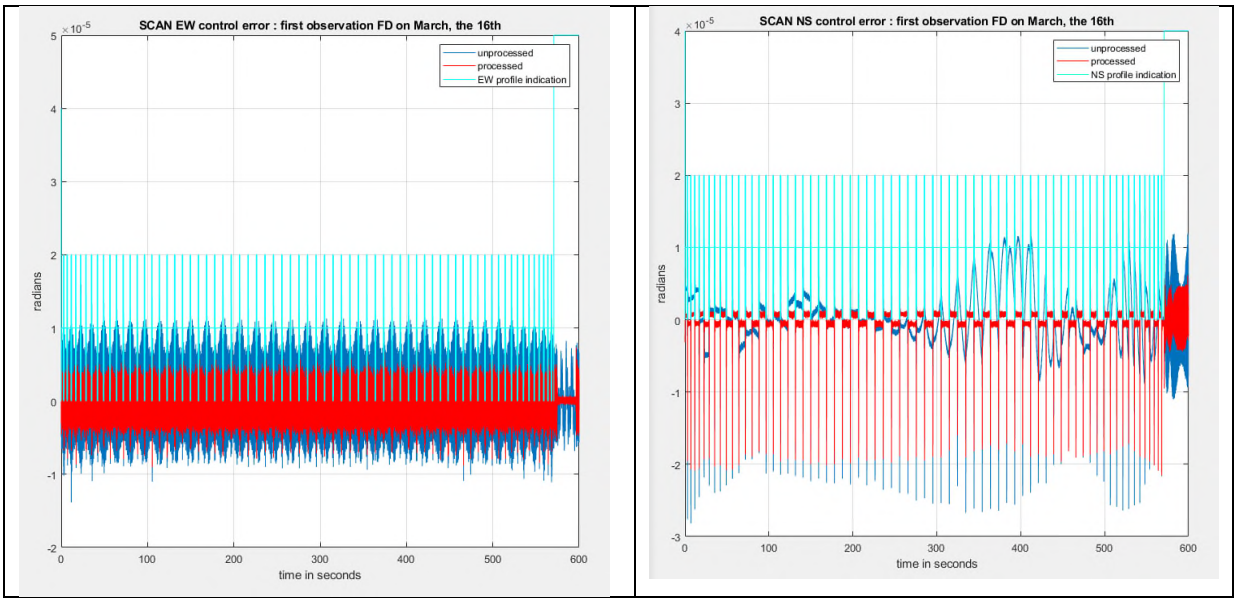

Figure 20. Scan attitude control error over a Full Disk

Then the APC has been enabled, the correct synchronization at 1ms checked as shown on Figure 21 where is plotted the torque send to the RW electronics and the Scan movement. Note that the RW electronics will react to the commanded torque following a first order profile with a time response equal to 100ms at 99% : the SCAN law acceleration profile has been designed to follow the same kind of behaviour in order to allow an efficient compensation.

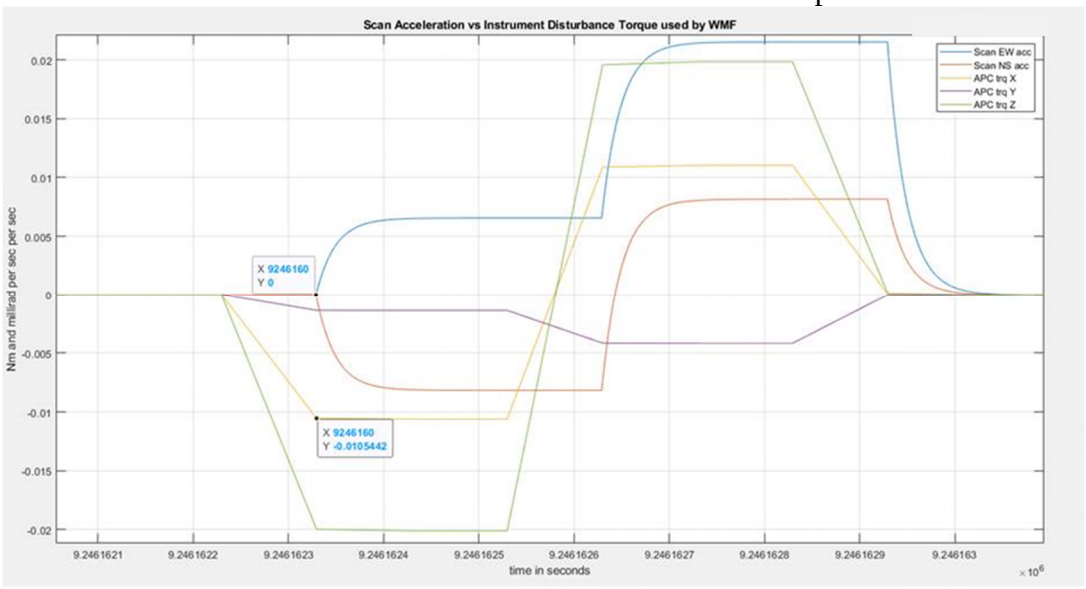

Figure 21. APC torque vs Scan acceleration

The beneficial effect on attitude is clearly visible: on figure 22 the APC has been enabled at 12:45, we note less excitation of the bending modes and smaller transient at each scan acceleration phase.

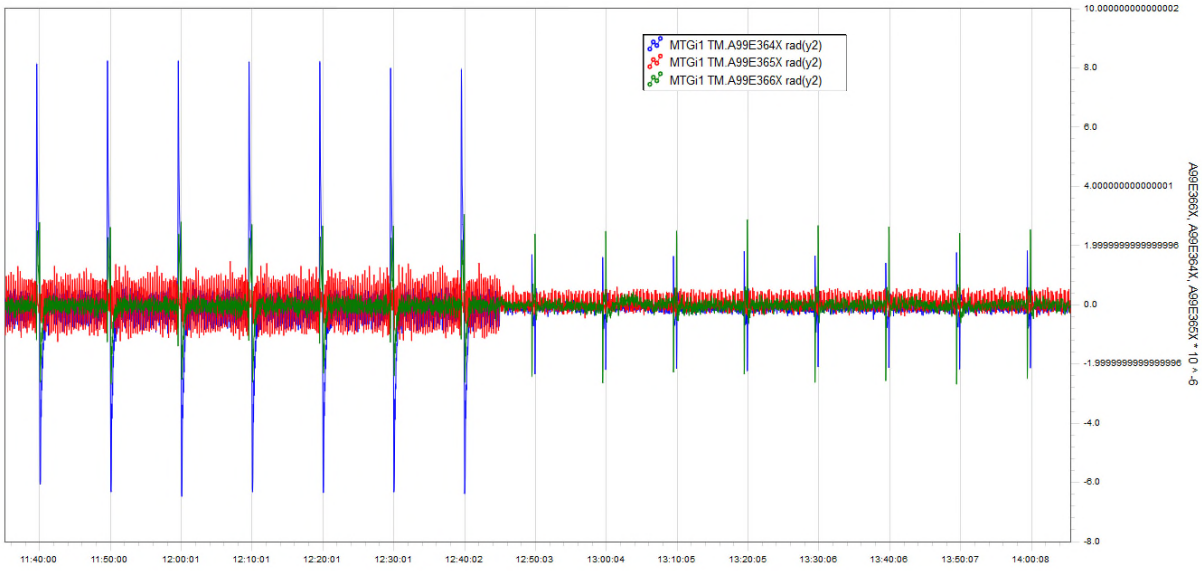

Figure 22. Impact of APC use on attitude control error (A99E364 = Z sat axis, A99E365 = Y sat axis, A99E366 = X sat axis)

6. Still to be done

The MTG commissioning phase is still in progress and should last up to the end of the Summer. At AOCS level, most of the functionalities have now been successfully tested even if some fine tunings shall still be concluded. At beginning of June, a North South orbit correction manoeuvre will be tested and then lastly a depointing manoeuvre in FPM will be commanded to observed with the FCI out of the Earth Disk in order to perform stray light calibration.

7. Conclusions

Thanks to these good performances reached by the attitude control and estimation in FPM, the main instrument of the MTG-I, FCI has taken its first pictures : the first official one was revealed to the 'World' on May the 4th and according to the specialists, its quality is amazing : it reveals a level of detail about the weather over Europe and Africa not previously possible from GEO orbit, giving more information about the clouds cloaking much of Europe and visible in the equatorial region of Africa and the Atlantic Ocean. Sand and sediment in the waters off Italy are also visible, as well as dust or smog being carried from south Asia. This degree of detail is not possible from the instruments on the Meteosat Second Generation satellites. The image on figure 23 was captured at 11:50 UTC on 18 March 2023.

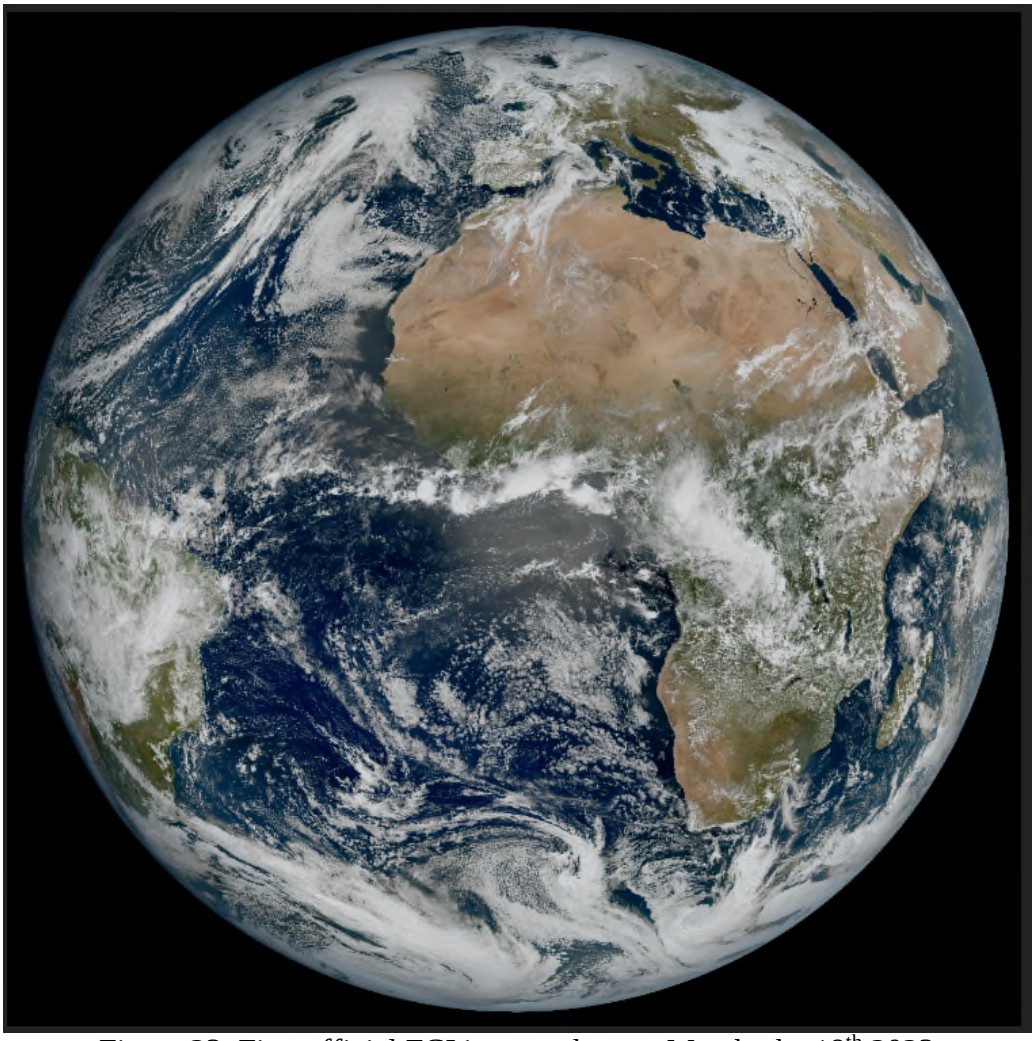

Figure 23. First official FCI image taken on March, the 18th 2023

8. Acknowledgments

The authors thank all the others colleagues in OHB, Thales Alenia Space France, ESA, EUMETSAT and TELESPAZIO for the valuable contributions provided during the LEOP and Commissioning phases.

9. References

[1] M. Battilana, L. Ascani, D. Bindel, M. Jacquemard, G. Rigot, B. Lübke-Ossenbeck, *Meteosat Third Generation AOCS overview*, 9th International ESA Conference on Guidance, Navigation & Control Systems, 2014

[2] L. Pirson, O. Rouat, N. Deslaef, D, Guichon, Y. Roche, *Meteosat Third Generation Fine Pointing Mode Design*, 9th International ESA Conference on Guidance, Navigation & Control Systems, 2014

[3] M. Battilana, L. Ascani, J. Habets, M. Jacquemard, G. Rigot, *Meteosat Third Generation: challenges at the end of the design phase*, 10th International ESA Conference on Guidance, Navigation & Control Systems, 2017